Communications in Computational Chemistry
Commun. Comput. Chem., Vol. 7, No. 4, 372–381
doi: 10.4208/cicc.2025.203.01
Regular Article

Theoretical Study on the Inhibition Mechanism of the Proteasome by Bortezomib

Yuwei Chen[1], Jinshuai Song[1,*],Yu Lan[1,2,3,*] and Donghui Wei[1,*]

[1]*College of Chemistry, and Pingyuan Laboratory, Zhengzhou University, Zhengzhou, Henan 450001, P. R. China;*

[2]*State Key Laboratory of Antiviral Drugs, and Pingyuan Laboratory, Henan Normal University, Xinxiang, Henan 453007, P. R. China;*

[3]*School of Chemistry and Chemical Engineering, Chongqing Key Laboratory of Chemical Theory and Mechanism, Chongqing University, Chongqing 401331, P. R. China.*

[*] Corresponding authors: jssong@zzu.edu.cn; LanYu@cqu.edu.cn; donghuiwei@zzu.edu.cn.

Received on 22 July 2025; Accepted on 12 September 2025

Abstract: Bortezomib can form covalent bonds with the proteasome to kill myeloma tumor cell, but the detailed covalent inhibition reaction mechanism remains unclear. In this study, we first established the parameters for boron atom in bortezomib and explored the possible reaction pathways of inhibition of the proteasome by bortezomib through molecular dynamics (MD) simulation and Quantum Mechanics/Molecular Mechanics (QM/MM) calculation. The computational results indicate that the most energetically favorable pathway includes two reaction steps. The first step involves a proton abstraction from the -OH group to -NH_2 group of Thr1 residue, which is coupled with the nucleophilic attack on the boron atom of bortezomib by the newly formed O^- ion. The second step is the proton transfer from the protonated -NH_3^+ group to one of the hydroxyl group connected to the boron atom, forming a bortezomib-proteasome complex associated with a water molecule coordinated with the boron atom. The rate-determining step of the inhibition reaction is the first step with an energy barrier of 19.1 kcal/mol, which is close to the activation energy of ~20.8 kcal/mol derived from kinetic experiments. This work provides detailed mechanistic insights for proteasome inhibition by the boron compounds.

Key words: bortezomib, proteasome, inhibition mechanism, QM/MM calculation.

1. Introduction

The proteasome is a large protein complex (2500 kDa) that regulates intracellular proteolysis. With a sedimentation coefficient of 26S as determined by density gradient centrifugation, it is also known as the 26S proteasome [1-3]. The 26S proteasome consists of the 19S regulatory particle and the 20S core particle, and many researches have shown that degradation can occur without the regulation of the 19S particle and can be mediated solely by the 20S proteasome, which is thus identified as the catalytic core of the proteasome [1,2,4-6]. As we all know, proteins in living cells are constantly being degraded and synthesized, and the proteasome generally plays an indispensable role in the cells for degrading misfolded and useless proteins into amino acids [7-9]. If the proteasome is inhibited, the cells will die quickly. Although scientists have not fully demonstrated the reasons why proteasome

inhibitors can selectively kill cancer cells while they are harmless to normal cells, this does not affect the potential applications of proteasome inhibitors as anti-tumor drugs [10-12]. Noteworthy, it has been discovered that proteasome inhibitors possess excellent anticancer activity, and have already begun to be applied in the medical field [13-15].

Up to now, a great number of inhibitors have been reported in the literature to inhibit the proteasome [16-23]. Based on their structural characteristics and different modes of action with the proteasome, they can be roughly divided into two main categories: covalent inhibitors and non-covalent inhibitors depicted in **Figure 1**. Covalent inhibitors include several types, such as aldehyde peptides [24-25], boronic acid peptides [26-29], β-lactones [20,30-32], vinyl sulfone peptides [33-35], and epoxyketones [36-38] and others [19]. Non-covalent inhibitors include cyclic peptide inhibitors (such as TMC-95A and its derivatives) [38-42].

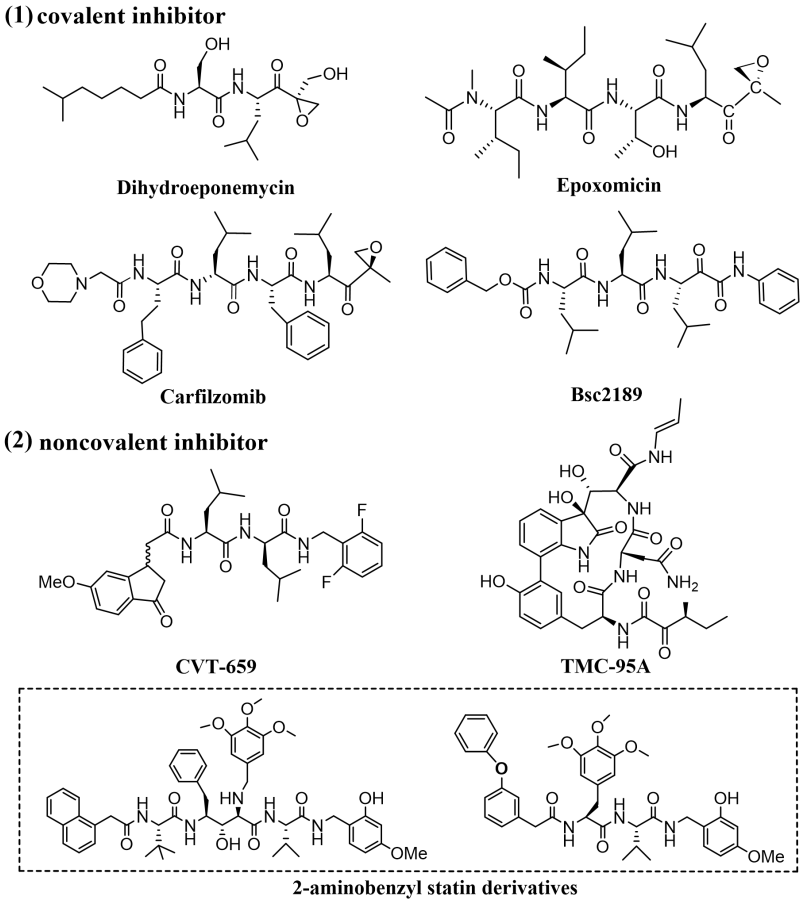

Figure 1. Examples of covalent and non-covalent inhibitors of proteasome.

Each of proteasome active site contains an N-terminal threonine (Thr1) residue, whose terminal amine serves as the general basis for Thr1-OH activation [3,43-45]. Then the activated Thr1-O^- ion can act as a nucleophile in proteasome-catalyzed hydrolysis of the peptide bond of the protein, and it can also attack the corresponding inhibitor molecules to form a covalent bond. Different types of inhibitors may have different covalent-binding modes and reaction mechanisms at the proteasome active site. For example, vinyl sulfone inhibitors (such as Z-L3VS) [46] form covalent bonds through nucleophilic attack by Thr1-O^- on the olefinic carbon, β-lactone inhibitors such as NPI-0047 [47] can react with Thr1-O^- to form covalent bonds. Peptide aldehyde inhibitors such as Ac-Leu-Leu-nLeu-al [48], form a hemiacetal bond between the aldehyde group and the Thr1-O^- at the active site depicted in **Figure 2**. For many years, scientists have studied several types of inhibition mechanism of proteasome through theoretical calculations [17,18,49-53]. However, the inhibition mechanism of some special types of covalent inhibitors such as bortezomib, remains to be unexplored in theory.

The proteasome inhibitor bortezomib has been approved by the U.S. Food and Drug Administration (FDA) in 2003 for the treatment of multiple myeloma [54,55]. It can inhibit the tumor activity by interacting with the proteasome. Although the catalytic rate constant of this reaction has been characterized [56], the fundamental reaction pathway remains unclear due to limitations in the parameters of boron atom during the computational process. This issue and our interest in mechanistic studies of proteasome prompt us to contribute this computational work on the bortezomib inhibition reaction. Based on the previous theoretical studies on the proteasome inhibition by other kinds of inhibitors [18,49], we have proposed a possible pathway for the bortezomib inhibition depicted in **Scheme 1**. The pathway involves intramolecular proton transfer of Thr1 in the proteasome coupled with B-O bond formation, and a second intramolecular proton transfer. In this work, we aim to clarify the detailed mechanism of the inhibition reaction of bortezomib and the rate-determining step of the reaction. In the

present study, we have explored the possible reaction steps of bortezomib inhibiting the proteasome through Molecular Dynamics (MD) simulation and Quantum Mechanics/Molecular Mechanics (QM/MM) calculation. Notably, QM/MM calculation are widely used to study enzyme reaction mechanism, and the computational results could clearly reveal the most favorable reaction pathway [57-60]. We believe this work should be useful for understanding the general mechanism of proteasome inhibition by using boron compounds.

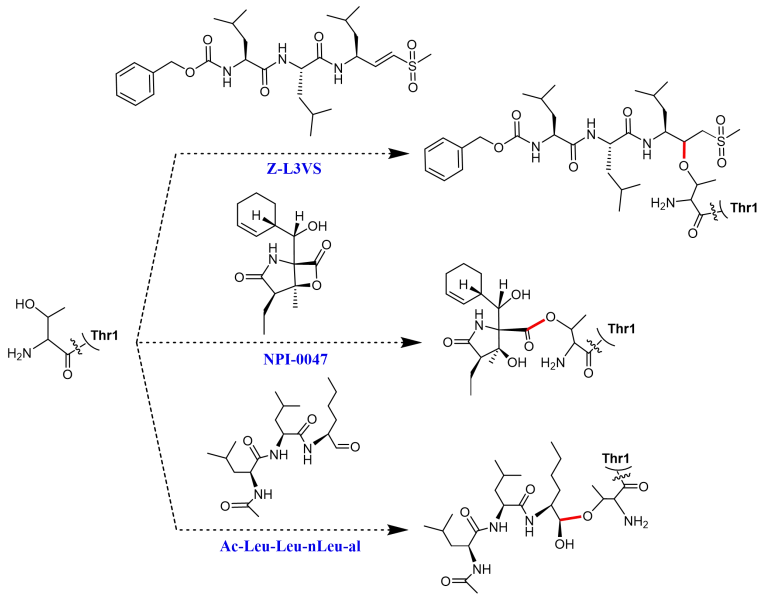

Figure 2. The inhibition reactions of proteasome by using three representative types of inhibitors including Z-L3VS, NPI-0047, and Ac-Leu-Leu-nLeu-al.

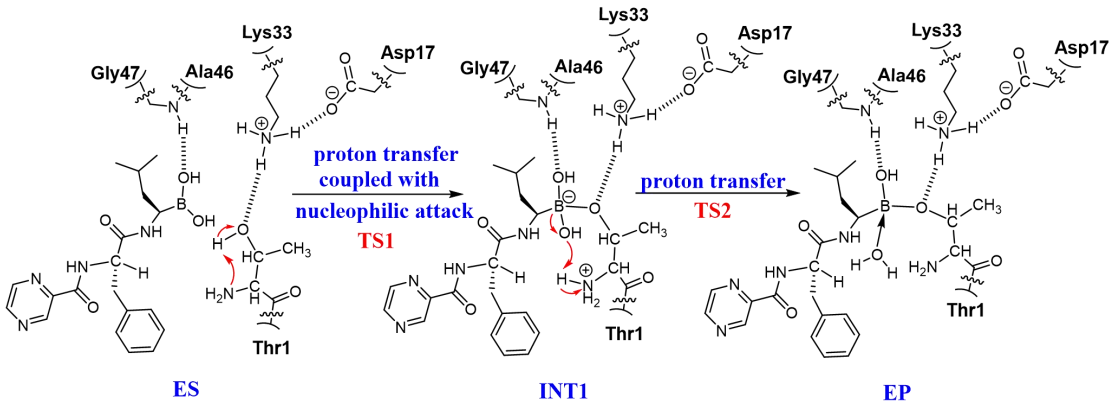

Scheme 1. Possible reaction pathway for bortezomib with proteasome.

2. Computational methods

2.1 Preparation of the initial Enzyme−Substrate structure

The initial model of the proteasome enzyme-substrate (ES) complex has been constructed based on the crystal structure (PDB ID: 2F16) [61], which is a polymeric structure comprising 28 chains in four stacked ring (**Figure 3**). The 20S proteasome is composed of 28 subunits arranged into four stacked rings (i.e. two β-rings in the middle and two α-rings on the sides), and each ring consists of seven subunits [45,62]. The β1, β2, and β5 subunits possess caspase-like (C-L), trypsin-like (T-L), and chymotrypsin-like (CT-L) activities, respectively [1,2,4,45,63-65]. Therefore, the proteasome has a total of six active sites. Referring to our previous work [18] on the inhibition reaction between epoxomicin and the proteasome, the β5 active site is located at the interface between the β5 and β6 subunits. By retaining only the two subunits (β5 and β6) as the initial structure of the ES complex, we prepared the model for subsequent molecular dynamics (MD) simulation. The atomic charges of the substrate used in the MD simulations and subsequent QM/MM calculation were restrained electrostatic potential (RESP) charges. The RESP charges for bortezomib were calculated at the HF/6-31G(d) level using the Gaussian 09 program [66]. In this study, we used the Visual Molecular Dynamics (VMD) program [67] as the visualization software for the MD simulation

configurations. The protein and bortezomib molecules were modeled using the Amber FF14SB [68] and Amber GAFF [69] force fields, respectively. Since the Amber force field can only recognize carbon, hydrogen, oxygen, nitrogen, phosphorus, sulfur, and halogens, we needed to develop parameters for boron. Based on the classical AMBER force field method developed by the Kollman [70,71] group and by referencing the three-point method established by our research group [72], we successfully fitted the parameters for boron, and the specific boron parameters are provided in **Supporting Information**. The tleap program was used to add all missing hydrogen atoms in the protein. The TIP3P model [73] was used for 22,696 water molecules, including solvation waters with 15 Å around the ES. By adding eight potassium ions as counterions to neutralize the reaction system, an initial system was obtained for subsequent molecular dynamics simulation. The entire MD simulation system comprises a total of 74,676 atoms. We have performed a 100 ns MD simulation, and more details about the MD simulation can be found in the previous work [18,74]. Overall, the MD simulation were performed using the GPU-accelerated version of the PMEMD module [75] in Amber20 software [76].

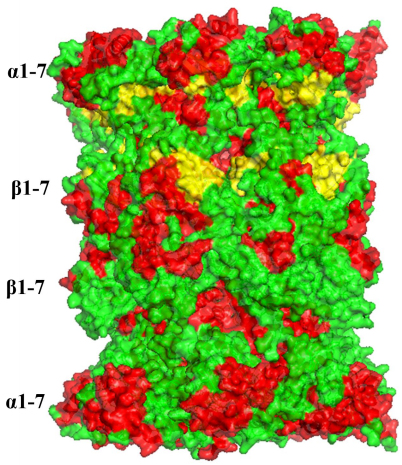

Figure 3. The 20S proteasome has a structure composed of 28 subunits arranged into four stacked rings.

2.2 QM/MM calculation

We selected the 193rd snapshot from the 100 ns MD simulation (with 10,000 frames in 100 ns) as the initial structure for the QM/MM calculation model. Based on the previous work [18,74], we thought the selected average structure in the equation MD should be proper for QM/MM calculations of proteasome reactions. As shown in **Figure S1**, we retained all 7,065 water molecules including a solvation shell of 12 Å around the ES complex in the QM/MM calculation. The QM region contained 75 atoms, which included a part of substrate bortezomib, and some atoms of the side chains Thr1, Asp17, Lys33 and Gly47. The selected QM region had a total charge of 0 and a spin multiplicity of 1. The QM/MM calculation were performed using ChemShell [77,78] as the interface program, which invoked the ORCA software [79-81] for quantum mechanical calculation in the QM region and DL_POLY [82,83] for molecular mechanical calculation in the MM region. To account for the polarization effects of the MM region on the QM region, an electronic embedding approach was employed. Hydrogen atoms were designated as the boundary atoms between the QM and MM regions. After scanning the bond length changes, the system's potential energy surface (PES) along the reaction coordinate was obtained. The dimer method implemented in the DL-FIND optimizer [84] was then used to optimize the transition state (TS) structure. Subsequently, frequency vibrational analysis was carried out on the obtained TS to verify its authenticity. The discussed Gibbs free energies have been obtained by Gibbs free energy corrections of the stationary points (SPs) calculated at the [B3LYP-D4/def2-SVP: Amber] level plus the single-point energy computed at the [B3LYP-D4/def2-TZVPP: Amber] level [85-88].

3. Results and discussion

3.1 MD simulation analyses

To determine whether the enzyme-substrate complex system under study had reached equilibrium, the root mean square deviation (RMSD) and root mean square fluctuation (RMSF) of the enzyme-substrate complex were calculated using the CPPTRAJ program [89], referencing the initial structure of the system. Plots of the RMSD and RMSF of the residue atoms in the enzyme-substrate complex system over time and as a function of residue number were generated. In **Figure 4A**, it was observed that during the 100 ns MD simulation, the RMSD values of the enzyme-substrate complex fluctuated within the range of 1.25-1.45 Å, indicating that the system had reached an equilibrium state over the course of the 100 ns MD simulation. In **Figure 4B**, the RMSF values of the complex ranged from 0.1 to 1.5 Å, suggesting that the overall conformational changes were minimal during the MD simulation. Many researchers have highlighted the importance of residues Asp17 and Lys33 when using proteasome inhibitors [45,52,53,65]. Asp17, Lys33, and Thr1 form a catalytic triad, and the ionization states of Asp17 and Lys33 influence each other due to strong electrostatic interactions [65]. In this study, a hydrogen bond interaction exists between deprotonated Asp17 and protonated Lys33, and Lys33 can form an N-H(Lys33)···O(Thr1) hydrogen bond with Thr1. During the MD simulation, it was observed that Gly47 can also form an N-H(Gly47)···O(bortezomib) hydrogen bond with bortezomib. To verify that the substrate can stably reside near the active site of the proteasome, we have tracked the distances of these three hydrogen bonds. As shown in **Figure 4C**, the hydrogen bond distance between Asp17 and Lys33 ranges from 1.65 to 2.25 Å, and the hydrogen bond distance between Lys33 and the reactive Thr1 ranges from 1.65 to 2.10 Å. The hydrogen bond distance between Gly47 and bortezomib ranges from 1.75 to 2.50 Å. These findings indicate that the hydrogen bond network near the active site can stably anchor bortezomib over the course of the 100 ns MD simulation. Additionally, it can be found that the average distance between B(bortezomib) and O(Thr1) during the 100 ns MD simulation is around 3.25 Å. (**Figure 4D**).

3.2 Possible mechanism

In **Scheme 1**, we considered a possible pathway for bortezomib inhibition as described. **Figure 5** shows the energy profile of the reaction pathway. For the fundamental reaction pathway, the first step involves an intramolecular proton transfer from the hydroxyl

hydrogen to the amino nitrogen of Thr1, while the negatively Thr1-O^- acts as a nucleophile to attack the boron atom of bortezomib. During the nucleophilic attack process, a new B-O covalent bond is formed in **INT1** through transition state **TS1** with an energy barrier of 19.1 kcal/mol. Moreover, it is worth noting that we have attempted but failed to find the stepwise transition state for the first step. However, the energy kept increasing to >41.9 kcal/mol during the energy scan along B-O bond process without the proton transfer, thus we can rule out this unreasonable sequence of reactions. More details can be found in the energy scan curve of **Figure S2** in **Supporting Information**. The second step involves another proton transfer from the protonated Thr1-NH_3^+ to B-OH group, forming a molecule of water coordinated with the B atom through transition state **TS2**. A coordination bond is formed between the oxygen atom of the water molecule and the boron atom, with a bond length of 1.63 Å. The B atom is confirmed to be in the tetrahedral coordination mode within the crystal structure (PDB ID: 2F16) [61]. It should be noted that the transition state **TS2** is 0.4 kcal/mol higher than the intermediate **INT1** without zero-point energy and thermal corrections, while the Gibbs free energy difference between the transition state **TS2** and the intermediate **INT1** becomes -0.8 kcal/mol with zero-point energy and thermal corrections. This indicates that this proton transfer step is a barrier-less process. Moreover, the inhibition of proteasome by bortezomib has confirmed that the entire inhibition process from **ES** to **EP** is endothermic with a value of 1.7 kcal/mol and should be reversible [90-92]. **Figure 6** illustrates that the distances of B (bortezomib)-O (Thr1), N-H (Lys33)···O (Thr1), N-H (Lys33)···O (Asp17), and N-H (Gly47)···O (bortezomib) in the transition state **TS1** are 2.18, 1.73, 1.65, and 1.92 Å, respectively. Whereas the distances of N-H (Lys33)···O (Thr1), N-H(Lys33)···O(Asp17), and N-H(Gly47)···O(bortezomib) in the transition state **TS2** are 1.74, 1.60, and 1.94 Å, respectively. During the process of proton transfer coupled with nucleophilic attack, the hydrogen bond distance between Lys33 and Thr1 changes from the initial 1.79 Å to 1.73 Å in transition state TS1. The distance is slightly shortened, and the interaction is enhanced, enabling Lys33 to stabilize the transition state TS1, with the hydrogen bond distance in the final intermediate INT1 being 1.72 Å. At the same time, the hydrogen bond between Asp17 and Lys33 increases from 1.57 Å to 1.65 Å in the transition state. While Lys33 stabilizes Thr1, it weakens the interaction with Asp17, and the hydrogen bond distance in INT1 is 1.62 Å. In the subsequent proton transfer process, the hydrogen bond distance between Lys33 and Thr1 changes from 1.72 Å to 1.74 Å in TS2, and the hydrogen bond distance in EP is 1.84Å. Meanwhile, the hydrogen bond between Asp17 and Lys33 changes from 1.62 Å to 1.60 Å in TS2, and the hydrogen bond distance in EP shortens to 1.55 Å. This could be due to the fact that the product has reached a stable state, leading to the enhanced interaction between Lys33 and Asp17.

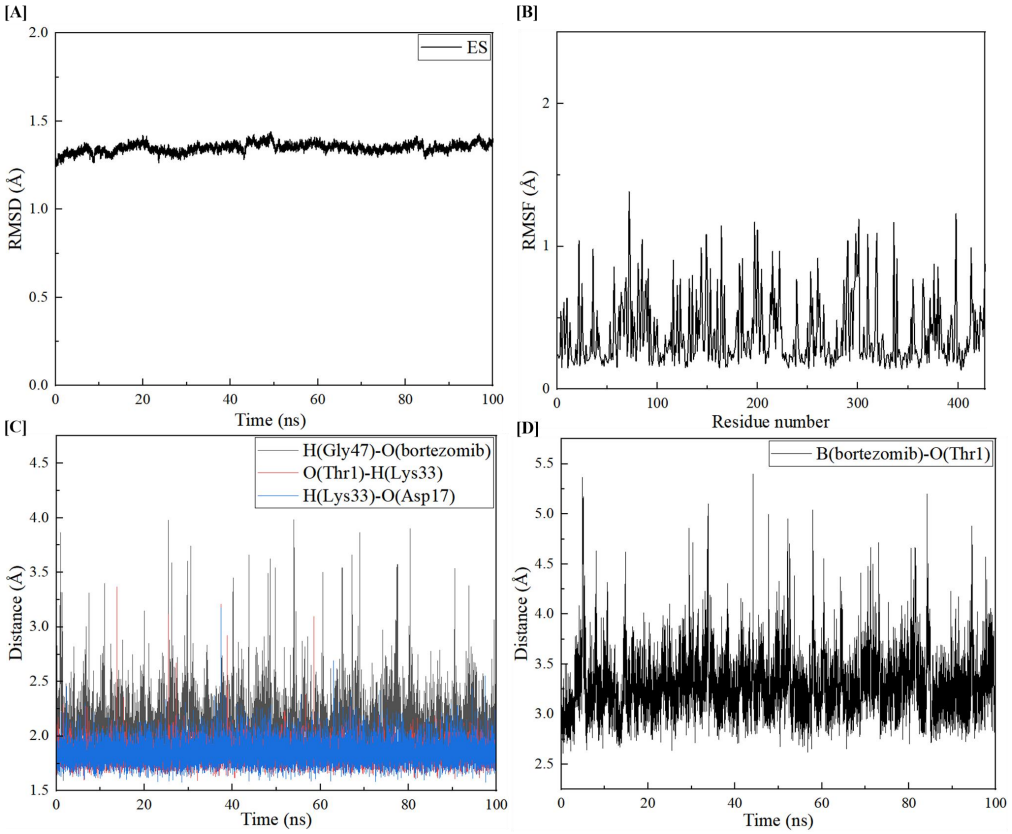

Figure 4. (A) RMSD values of all atoms of the whole system with respect to the corresponding starting structures for the entire MD simulations of the protein and substrates. (B) RMSF values of all residues (numbers 1−426 are residues, and number 427 is substrate) referenced to the average structure of all atoms in the enzyme−substrate complex during equilibrium simulations. (C) Changes of distances associated with H(Gly47)-O(bortezomib), O (Thr1)-H(Lys33), H(Lys33)-O(Asp17) during the MD simulation. (D) Changes of distances associated with B (bortezomib)-O(Thr1) during the MD simulation.

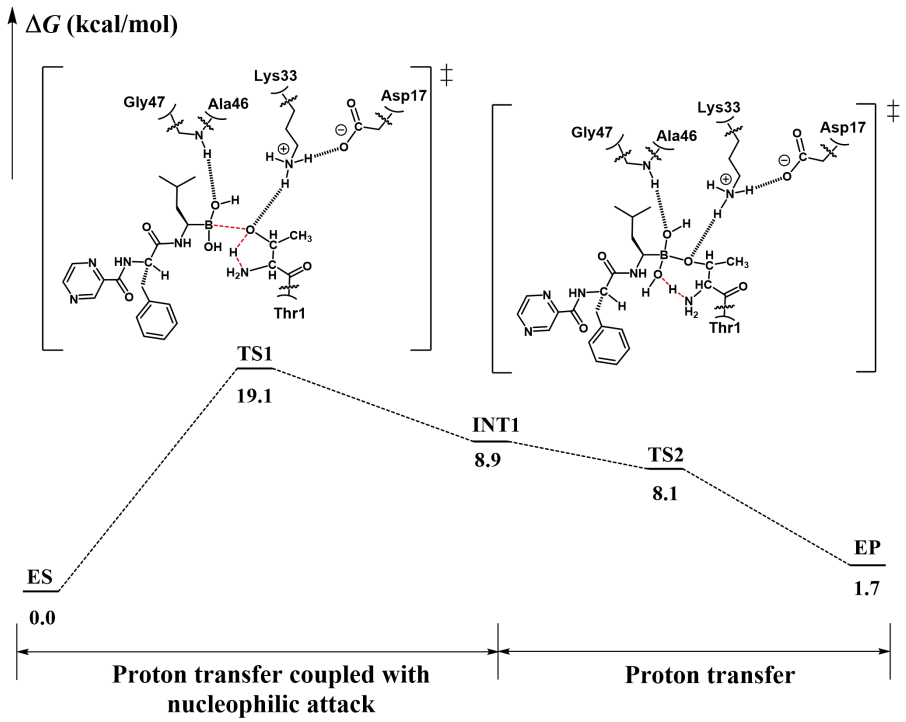

Figure 5. Relative Gibbs free energy profile for the inhibition pathway of the proteasome by bortezomib.

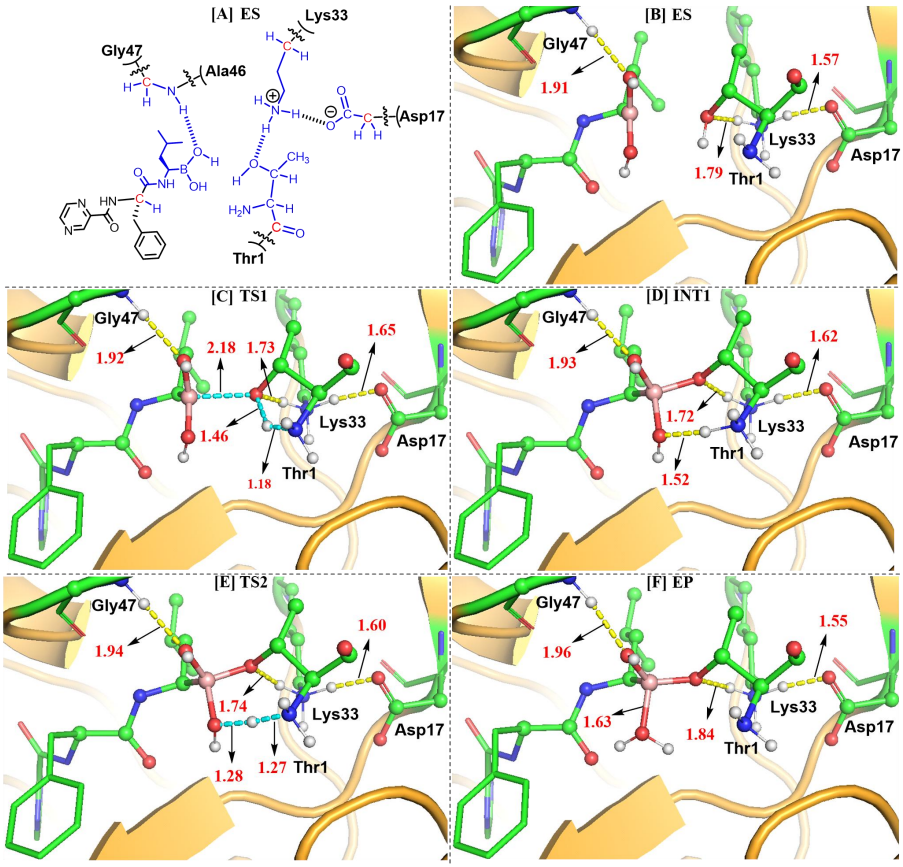

Figure 6. (A) Setting of the QM (blue), MM (black), and boundary atoms (red). (B-F) 3D structures of **ES**, **TS1**, **INT1**, **TS2**, and **EP**. For clarity, only the hydrogen atoms attached to heavy atoms of residues that can form hydrogen bonds in the active center of the residue and the hydrogen atoms on the hydroxyl group of the substrate are shown. Carbon, oxygen, nitrogen, and hydrogen atoms are colored in green, red, blue, and white, respectively. The QM and MM atoms are respectively shown in ball-and-stick and cartoon styles. The cyan and yellow dashed lines represent the distance of the transition states and hydrogen bonds (Distance in Å).

According to the reported experimental data, the observed rate constant (k_{obs}) is 0.2 min^{-1} [56], which corresponds to an energy barrier of 20.8 kcal/mol at 298.15 K based on transition state theory. Our computational results indicate that the energy barrier through **TS1** (19.1 kcal/mol) is close to the experimentally determined energy barrier. As concerned as above, the first step is the rate-determining step of the reaction, and the computational results are kinetically reasonable. We also selected the 2146th snapshot as initial structure for the QM/MM calculation, and the computed results summarized in **Table S2** are also close to the activation energy of approximately 20.8 kcal/mol derived from kinetic experiments.

4. Conclusion

By fitting the parameters of bortezomib using the three-point method, we have investigated the detailed inhibition mechanism of proteasome by bortezomib through MD simulations and QM/MM calculation for the first time. The calculated results of the MD simulation indicate that the parameters for bortezomib have been successfully established. Specifically, the hydrogen bond network among the three key residues including Lys33, Asp17, and Thr1 can be formed and plays an important role in the inhibition reaction. Further QM/MM calculated results indicates that intramolecular proton transfer is coupled with nucleophilic attack to bortezomib to form a tetrahedral complex, which is followed by a proton transfer to form a more stable intermediate in the fundamental reaction pathway. Noteworthy, the inhibition reaction has been confirmed to be slightly endothermic, demonstrating the bortezomib is a kind of reversible inhibitor. This theoretical work helps in understanding the complete inhibition mechanism of 20S proteasome by the boron-containing small-molecule inhibitors, and thus provides a theoretical basis for the rational design of boron-containing drug molecules.

Supporting information

Please see the Supporting Information in the attachment. https://global-sci.com/storage/self-storage/cicc-2025-203-1-R1-si.pdf.

Acknowledgments

We acknowledge financial support from the Outstanding Youth Science Foundation Project of Henan Province (No. 252300421039), the Key Project of the Joint Fund for Science and Technology Research and Development in Henan Province (No. 232301420008), and the National Natural Science Fund of China (Nos. 22473100, 21773214 and 21303167).

References

[1] Davis C., Spaller B.S. and Matouschek A., Mechanisms of substrate recognition by the 26S proteasome. *Curr. Opin. Struc. Biol.,* **67** (2021), 161–169.

[2] Sahu I. and Glickman M.H., Proteasome in action: substrate degradation by the 26S proteasome. *Biochem. Soc. Trans.,* **49** (2021), 629–644.

[3] Unno M., Mizushima T., Morimoto Y., Tomisugi Y., Tanaka K., Yasuoka N. and Tsukihara T., The structure of the mammalian 20S proteasome at 2.75 Å resolution. *Structure,* **10** (2002), 609–618.

[4] Zhang P.-Y., Wang C.-C., Jia W., Jiang C.-Z. and Fu D.-Q., 26S proteasome subunit SlPBB2 regulates fruit development and ripening in tomato. *J. Agr. Food. Chem.,* **73** (2025), 2991–2998.

[5] Arkinson C., Dong K.C., Gee C.L., Costello S.M., Soe A.C., Hura G.L. and Martin A., NUB1 traps unfolded FAT10 for ubiquitin-independent degradation by the 26S proteasome. *Nat. Struct. Mol. Biol.,* **32** (2025), 1752–1765.

[6] Deshmukh F.K., Yaffe D., Olshina M.A., Ben-Nissan G. and Sharon M., The contribution of the 20S proteasome to proteostasis. *Biomolecules,* **9** (2019), 190.

[7] Lefaki M., Papaevgeniou N. and Chondrogianni N., Redox regulation of proteasome function. *Redox Biol.,* **13** (2017), 452–458.

[8] Yilmaz S., Bedir E. and Kirmizibayrak P.B., The role of cycloastragenol at the intersection of NRF2/ARE, telomerase, and proteasome activity. *Free Radical Bio. Med.,* **188** (2022), 105–116.

[9] Atta H., Kassem D.H., Kamal M.M. and Hamdy N.M., Harnessing the ubiquitin proteasome system as a key player in stem cell biology. *Biofactors,* **51** (2025), e2157.

[10] Rahimi N., The evolution and diversification of proteasome inhibitors in cancer and beyond. *ChemRxiv.,* (2025).

[11] He H.-J., Liu S., Wu D.-F. and Xu B., Enzymatically formed peptide assemblies sequestrate proteins and relocate inhibitors to selectively kill cancer cells. *Angew. Chem. Int. Ed.,* **59** (2020), 16445.

[12] Xu M., Zhang Z.-Q., He X.-Y., Zhang P.-X., Zhang H.-Y., Xia Y.-X., Zhou J.-M., Liu J., Ye X.-T. and Liu J.-Q., Mechanistic insights into proteasome inhibitor MG132 induced apoptosis in melanoma A375 cells. *Sci. Rep.,* **15** (2025), 14731.

[13] Sin C.-F. and Man P.M., The role of proteasome inhibitors in treating acute lymphoblastic leukaemia. *Front. Oncol.,* **11** (2021).

[14] Weir P., Donaldson D., McMullin M.F. and Crawford L., Metabolic alterations in multiple myeloma: from oncogenesis to proteasome inhibitor resistance. *Cancers,* **15** (2023), 1682.

[15] Marzan M., Oishee N.N., Olatunji A.O., Shourav A.H., Noor R.E., Astalos A.J., Leahy J.W. and Acevedo-Duncan M., Proteasome inhibitor MG-132 and PKC-ι-specific inhibitor ICA-1S degrade mutant p53 and induce apoptosis in ovarian cancer cell lines. *Int. J. Mol. Sci.,* **26** (2025), 3035.

[16] Mihalovits L.M., Ferenczy G.G. and Keserű G.M., Mechanistic and thermodynamic characterization of oxathiazolones as potent and selective covalent immunoproteasome inhibitors. *Comput. Struct. Biotec.,* **19** (2021), 4486–4496.

[17] Serrano-Aparicio N., Świderek K. and Moliner V., Theoretical study of the inhibition mechanism of human 20S proteasome by dihydroeponemycin. *Eur. J. Med. Chem.,* **164** (2019), 399–407.

[18] Wei D.-H., Lei B.-L., Tang M.-S. and Zhan C.-G., Fundamental reaction pathway and free energy profile for inhibition of proteasome by epoxomicin. *J. Am. Chem. Soc.,* **134** (2012), 10436–10450.

[19] Trivella D.B.B., Pereira A.R., Stein M.L., Kasai Y., Byrum T., Valeriote F.A., Tantillo D.J., Groll M., Gerwick W.H. and

Moore B.S., Enzyme inhibition by hydroamination: design and mechanism of a hybrid carmaphycin-syringolin enone proteasome inhibitor. *Cell Chem. Biol.,* **21** (2014), 782–791.

[20] Groll M., Nguyen H., Vellalath S. and Romo D., (−)-Homosalinosporamide A and its mode of proteasome inhibition: an X-ray crystallographic study. *Mar. Drugs,* **16** (2018), 240.

[21] Blackburn C., Gigstad K.M., Hales P., Garcia K., Jones M., Bruzzese F.J., Barrett C., Liu J.X., Soucy T.A., Sappal D.S., Bump N., Olhava E.J., Fleming P., Dick L.R., Tsu C., Sintchak M.D. and Blank J.L., Characterization of a new series of non-covalent proteasome inhibitors with exquisite potency and selectivity for the 20S β5-subunit. *Biochem. J.,* **431** (2010), 433.

[22] Zhuang R.-X., Gao L.-X., Lv X.-Q., Xi J.-J., Sheng L., Zhao Y.-M., He R.-Y., Hu X.-B., Shao Y.-D., Pan X.-W., Liu S.-R., Huang W.-W., Zhou Y.-B., Li J. and Zhang J.-K., Exploration of novel piperazine or piperidine constructed non-covalent peptidyl derivatives as proteasome inhibitors. *Eur. J. Med. Chem.,* **126** (2017), 1056–1070.

[23] Serrano-Aparicio N., Moliner V. and Świderek K., On the origin of the different reversible characters of Salinosporamide A and Homosalinosporamide A in the covalent inhibition of the human 20S proteasome. *ACS Catal.,* **11** (2021), 11806–11819.

[24] Wilson D.L., Meininger I., Strater Z., Steiner S., Tomlin F., Wu J., Jamali H., Krappmann D. and Götz M.G., Synthesis and evaluation of macrocyclic peptide aldehydes as potent and selective inhibitors of the 20S proteasome. *ACS Med. Chem. Lett.,* **7** (2016), 250–255.

[25] Löwe J., Stock D., Jap B., Zwickl P., Baumeister W. and Huber R., Crystal structure of the 20S proteasome from the archaeon T. acidophilum at 3.4 Å resolution. *Science,* **268** (1995), 533–539.

[26] Sogbein O., Paul P., Umar M., Chaari A., Batuman V. and Upadhyay R., Bortezomib in cancer therapy: mechanisms, side effects, and future proteasome inhibitors. *Life. Sci.,* **358** (2024), 123125.

[27] Tan C.R.C., Abdul-Majeed S., Cael B. and Barta S.K., Clinical pharmacokinetics and pharmacodynamics of bortezomib. *Clin. Pharmacokinet,* **58** (2019), 157–168.

[28] Naumann I., Kappler R., Schweinitz D., Michael K., Debatin and Fulda S., Bortezomib primes neuroblastoma cells for TRAIL-induced apoptosis by linking the death receptor to the mitochondrial pathway. *Clin. Cancer. Res.,* **17** (2011), 3204–3218.

[29] Piperdi B., Ling Y.-H., Liebes L., Muggia F. and Perez-Soler R., Bortezomib: understanding the mechanism of action. *Mol. Cancer Ther.,* **10** (2011), 2029–2030.

[30] Wolf F., Bauer J.S., Bendel T.M., Kulik A., Kalinowski J., Gross H. and Kaysser L., Biosynthesis of the β-lactone proteasome inhibitors belactosin and cystargolide. *Angew. Chem. Int. Ed.,* **56** (2017), 6665.

[31] Groll M., Balskus E.P. and Jacobsen E.N., Structural analysis of spiro β-lactone proteasome inhibitors. *J. Am. Chem. Soc.,* **130** (2008), 14981–14983.

[32] Nett M., Gulder T.A.M., Kale A.J., Hughes C.C. and Moore B.S., Function-Oriented biosynthesis of β-lactone proteasome inhibitors in *Salinispora tropica*. *J. Med. Chem.,* **52** (2009), 6163–6167.

[33] Xin B.-T., de Bruin G., Plomp J.-W., Florea B.I., van der Marel G.A. and Overkleeft H.S., Incorporation of the constrained peptidomimetic 5-methylpyridin-2-one into peptide vinyl sulfones and peptide epoxyketones is detrimental for proteasome inhibition. *Eur. J. Org. Chem.,* **2016** (2016), 1132–1144.

[34] Overkleeft H.S., Bos P.R., Hekking B.G., Gordon E.J., Ploegh H.L. and Kessler B.M., Solid phase synthesis of peptide vinyl sulfone and peptide epoxyketone proteasome inhibitors. *Tetrahedron Lett.,* **41** (2000), 6005–6009.

[35] Steverding D., Spackman R.W., Royle H.J. and Glenn R.J., Trypanocidal activities of trileucine methyl vinyl sulfone proteasome inhibitors. *Parasitol Res.,* **95** (2005), 73–76.

[36] Almaliti J., Fajtová P., Calla J., LaMonte G.M., Feng M., Rocamora F., Ottilie S., Glukhov E., Boura E., Suhandynata R.T., Momper J.D., Gilson M.K., Winzeler E.A., Gerwick W.H. and O'Donoghue A.J., Development of potent and highly selective epoxyketone-based plasmodium proteasome inhibitors. *Chem. Eur. J.,* **29** (2023), e202203958.

[37] Zeng G., Xu G.-Ya., Gao L.-X., Zheng X.-L., Chi X.-L., Shen Z-Y., Cao Y., Xi J.-J., Che J.-X., Dong X.-W., Shi Y.-L., Ma J.-Y., Zhang C., Zeng L.-H., Zhu H.-J., Shao J.-A., Zhou Y.-B., Li J. and Zhang J.-K., Development of novel epoxyketone macrocyclic peptidyl proteasome inhibitors through OPA-mediated one-step cyclization of unprotected peptides. *Bioorg. Chem.,* **156** (2025), 108180.

[38] Götz M.G., Godwin K., Price R., Dorn R., Merrill-Steskal G., Klemmer W., Hansen H., Produturi G., Rocha M., Palmer M., Molacek L., Strater Z. and Groll M., Macrocyclic oxindole peptide epoxyketones—A comparative study of macrocyclic inhibitors of the 20S proteasome. *ACS Med. Chem. Lett.,* **15** (2024), 533–539.

[39] McDaniel T.J., Lansdell T.A., Dissanayake A.A., Azevedo L.M., Claes J., Odom A.L. and Tepe J.J., Substituted quinolines as noncovalent proteasome inhibitors. *Bioorgan. Med. Chem.,* **24** (2016), 2441–2450.

[40] Tatar I., Uysal S., Yilmaz S., Tarikogullari A.H., Kirmizibayrak B.P. and Soyer Z., Design, synthesis, and biological evaluation of some novel naphthoquinone–glycine/β-alanine anilide derivatives as noncovalent proteasome inhibitors. *Chem. Biol. Drug Des.,* **101** (2023), 1283–1298.

[41] Inoue M., Zhai H.-F., Sakazaki H., Furuyama H., Fukuyama Y. and Hirama M., TMC-95A, a reversible proteasome inhibitor, induces neurite outgrowth in PC12 cells. *Bioorg. Med. Chem. Lett.,* **14** (2004), 663–665.

[42] Groll M., Koguchi Y., Huber R. and Kohno J., Crystal structure of the 20S proteasome: TMC-95A complex: a non-covalent proteasome inhibitor. *J. Mol. Biol.,* **311** (2001), 543–548.

[43] Brannigan J.A., Dodson G., Duggleby H.J., Moody P.C., Smith J.L., Tomchick D.R. and Murzin A.G., A protein catalytic framework with an N-terminal nucleophile is capable of self-activation. *Nature,* **378** (1995), 416–419.

[44] Zhang H.-X., Zhou C.-Y., Mohammad Z. and Zhao J.-H., Structural basis of human 20S proteasome biogenesis. *Nat. Commun.,* **15** (2024), 8184.

[45] Fung D., Razi A., Pandos M., Velez B., Perez E.F., Adams L., Rawson S., Walsh J.R. and Hanna J., Evidence supporting a catalytic pentad mechanism for the proteasome and other N-

terminal nucleophile enzymes. *Nat. Commun.,* **16** (2025), 2949.

[46] Bogyo M., McMaster J.S., Gaczynska M., Tortorella D., Goldberg A.L. and Ploegh H., Covalent modification of the active site threonine of proteasomal β subunits and the *Escherichia coli* homolog HslV by a new class of inhibitors. *Proc. Natl. Acad. Sci.,* **94** (1997), 6629–6634.

[47] Groll M., Huber R. and Potts B.C.M., Crystal structures of salinosporamide A (NPI-0052) and B (NPI-0047) in complex with the 20S proteasome reveal important consequences of β-lactone ring opening and a mechanism for irreversible binding. *J. Am. Chem. Soc.,* **128** (2006), 5136–5141.

[48] Marques A.J., Palanimurugan R., Matias A.C., Ramos P.C. and Dohmen R.J., Catalytic mechanism and assembly of the proteasome. *Chem. Rev.,* **109** (2009), 1509–1536.

[49] Wei D.-H., Tang M.-S. and Zhan C.-G., Fundamental reaction pathway and free energy profile of proteasome inhibition by syringolin A (SylA). *Org. Biomol. Chem.,* **13** (2015), 6857–6865.

[50] Mondal D. and Warshel A., Exploring the mechanism of covalent inhibition: simulating the binding free energy of α-ketoamide inhibitors of the main protease of SARS-CoV-2. *Biochemistry,* **59** (2020), 4601–4608.

[51] Ferrer S., Moliner V. and Świderek K., Electrostatic preorganization in three distinct heterogeneous proteasome β-subunits. *ACS Catal.,* **14** (2024), 15237–15249.

[52] Serrano-Aparicio N., Moliner V. and Świderek K., Nature of irreversible inhibition of human 20S proteasome by salinosporamide A: the critical role of Lys–Asp dyad revealed from electrostatic effects analysis. *ACS Catal.,* **11** (2021), 3575–3589.

[53] Zhou J., Sang X.-H., Wang J., Xu Y., An J., Chu Z.-T., Saha A., Warshel A. and Huang Z.-W., Elucidation of the α-ketoamide inhibition mechanism: revealing the critical role of the electrostatic reorganization effect of Asp17 in the active site of the 20S proteasome. *ACS Catal.,* **13** (2023), 14368–14376.

[54] Yang H.-J., Chen X., Li K., Cheaito H., Yang Q.-Q., Wu G.-J., Liu J.-B. and Dou P., Repurposing old drugs as new inhibitors of the ubiquitin-proteasome pathway for cancer treatment. *Semin. Cancer Biol.,* **68** (2021), 105–122.

[55] Richardson P.G., Sonneveld P., Schuster M.W., Irwin D., Stadtmauer E.A., Facon T., Harousseau J.L., Ben-Yehuda D., Lonial S., Goldschmidt H., Reece D., San-Miguel J.F., Blade J., Boccadoro M., Cavenagh J., Dalton W.S., Boral A.L., Esseltine D.L., Porter J.B., Schenkein D. and Anderson K.C., Bortezomib or high-dose dexamethasone for relapsed multiple myeloma. *New Engl. J. Med.,* **352** (2005), 2487–2498.

[56] Hasinoff B.B. and Patel D., Myocyte-damaging effects and binding kinetics of boronic acid and epoxyketone proteasomal-targeted drugs. *Cardiovasc. Toxicol.,* **18** (2018), 557–568.

[57] Zhou T.-P., Feng J.-Q., Wang Y.-C., Li S.-Y. and Wang B.-J., Substrate conformational switch enables the stereoselective dimerization in P450 NascB: insights from molecular dynamics simulations and quantum mechanical/molecular mechanical calculations. *JACS Au,* **4** (2024), 1591–1604.

[58] Wang Q.-Q., Song J.-S. and Wei D.-H., Origin of chemoselectivity of halohydrin dehalogenase-catalyzed epoxide ring-opening reactions. *J. Chem. Inf. Model.,* **64** (2024), 4530–4541.

[59] Senn H.M. and Thiel W., QM/MM methods for biomolecular systems. *Angew. Chem. Int. Ed.,* **48** (2009), 1198–1229.

[60] Fu Y.-Z., Yu J., Fan F.-F., Wang B.-J. and Cao Z.-X., Elucidating the enzymatic mechanism of dihydrocoumarin degradation: insight into the functional evolution of methyl-parathion hydrolase from QM/MM and MM MD simulations. *J. Phys. Chem. B,* **128** (2024), 5567–5575.

[61] Groll M., Berkers C.R., Ploegh H.L. and Ovaa H., Crystal structure of the boronic acid-based proteasome inhibitor bortezomib in complex with the yeast 20S proteasome. *Structure,* **14** (2006), 451–456.

[62] Wei D.-H., Fang L., Tang M.-S. and Zhan C.-G., Fundamental reaction pathway for peptide metabolism by proteasome: insights from first-principles quantum mechanical/molecular mechanical free energy calculations. *J. Phys. Chem. B,* **117** (2013), 13418–13434.

[63] Pepelnjak M., Rogawski R., Arkind G., Leushkin Y., Fainer I., Ben-Nissan G., Picotti P. and Sharon M., Systematic identification of 20S proteasome substrates. *Mol. Syst. Biol.,* **20** (2024), 403–427.

[64] Yu Z.-L., Yu Y.-D., Wang F., Myasnikov A.G., Coffino P. and Cheng Y.-F., Allosteric coupling between α-rings of the 20S proteasome. *Nat. Commun.,* **11** (2020), 4580.

[65] Huber E.M., Heinemeyer W., Li X., Arendt C.S., Hochstrasser M. and Groll M., A unified mechanism for proteolysis and autocatalytic activation in the 20S proteasome. *Nat. Commun.,* **7** (2016), 10900.

[66] Frisch M.J., Trucks G.W., Schlegel H.B., Scuseria G.E., Robb M.A., Cheeseman J.R., Scalmani G., Barone V., Petersson G.A., Nakatsuji H., Li X., Caricato M., Marenich A.V., Bloino J., Janesko B.G., Gomperts R., Mennucci B., Hratchian H.P., Ortiz J.V., Izmaylov A.F., Sonnenberg J.L., Williams-Young D., Ding F., Lipparini F., Egidi F., Goings J., Peng B., Petrone A., Henderson T., Ranasinghe D., Zakrzewski V.G., Gao J., Rega N., Zheng G., Liang W., Hada M., Ehara M., Toyota K., Fukuda R., Hasegawa J., Ishida M., Nakajima T., Honda Y., Kitao O., Nakai H., Vreven T., Throssell K., Montgomery J.A. Jr., Peralta J.E., Ogliaro F., Bearpark M.J., Heyd J.J., Brothers E.N., Kudin K.N., Staroverov V.N., Keith T.A., Kobayashi R., Normand J., Raghavachari K., Rendell A.P., Burant J.C., Iyengar S.S., Tomasi J., Cossi M., Millam J.M., Klene M., Adamo C., Cammi R., Ochterski J.W., Martin R.L., Morokuma K., Farkas O., Foresman J.B. and Fox D.J., Gaussian 09, Revision B.01. Gaussian, Inc., Wallingford CT, 2010.

[67] Humphrey W., Dalke A. and Schulten K., VMD: visual molecular dynamics. *J. Mol. Graph.,* **14** (1996), 33–38.

[68] Maier J.A., Martinez C., Kasavajhala K., Wickstrom L., Hauser K.E. and Simmerling C., ff14SB: improving the accuracy of protein side chain and backbone parameters from ff99SB. *J. Chem. Theory Comput.,* **11** (2015), 3696–3713.

[69] Wang J., Wolf R.M., Caldwell J.W., Kollman P.A. and Case D.A., Development and testing of a general amber force field. *J. Comput. Chem.,* **25** (2004), 1157–1174.

[70] Weiner S.J., Kollman P.A., Case D.A., Singh U.C., Ghio C., Alagona G., Profeta S. and Weiner P., A new force field for molecular mechanical simulation of nucleic acids and proteins. *J. Am. Chem. Soc.,* **106** (1984), 765–784.

[71] Cornell W.D., Cieplak P., Bayly C.I., Gould I.R., Merz K.M., Ferguson D.M., Spellmeyer D.C., Fox T., Caldwell J.W. and Kollman P.A., A second generation force field for the simulation of proteins, nucleic acids, and organic molecules. *J. Am. Chem. Soc.,* **117** (1995), 5179–5197.

[72] Zhu Y., Wang Y., Chen G. and Zhan C.-G., A three-point method for evaluations of amber force field parameters: an application to copper-based artificial nucleases. *Theor. Chem. Acc.,* **122** (2009), 167–178.

[73] Jorgensen W., Chandrasekhar J., Madura J., Impey R. and Klein M., Comparison of simple potential functions for simulating liquid water. *J. Chem. Phys.,* **79** (1983), 926–935.

[74] Lei B.-L., Abdul Hameed M.D., Hamza A., Wehenkel M., Muzyka J.L., Yao X.-J., Kim K.-B. and Zhan C.-G., Molecular basis of the selectivity of the immunoproteasome catalytic subunit LMP2-specific inhibitor revealed by molecular modeling and dynamics simulations. *J. Phys. Chem. B,* **114** (2010), 12333–12339.

[75] Salomon-Ferrer R., Götz A.W., Poole D., Le Grand S. and Walker R.C., Routine microsecond molecular dynamics simulations with AMBER on GPUs. 2. Explicit solvent particle mesh Ewald. *J. Chem. Theory Comput.,* **9** (2013), 3878–3888.

[76] Case D.A., Belfon K., Ben-Shalom I.Y., Brozell S.R., Cerutti D.S., Cheatham T.E., Cruzeiro V.W.D., Darden T.A., Duke R.E., Giambasu G., Gilson M.K., Gohlke H., Goetz A.W., Harris R., Izadi S., Kasavajhala K., Kovalenko A., Krasny R., Kurtzman T., Lee T.S., LeGrand S., Li P., Lin C., Liu J., Luchko T., Luo R., Man V., Merz K.M., Miao Y., Mikhailovskii O., Monard G., Nguyen H., Onufriev A., Pan F., Pantano S., Qi R., Roe D.R., Roitberg A., Sagui C., Schott-Verdugo S., Shen J., Simmerling C.L., Skrynnikov N., Smith J., Swails J., Walker R.C., Wang J., Wilson L., Wolf R.M., Wu X., York D.M. and Kollman P.A., AMBER 2020. University of California, San Francisco, 2020.

[77] Mitchell J.B.O., Machine learning methods in chemoinformatics. *WIREs Comput. Mol. Sci.,* **4** (2014), 468–481.

[78] Sherwood P., de Vries A.H., Guest M.F., Schreckenbach G., Catlow C.R.A., French S.A., Sokol A.A., Bromley S.T., Thiel W., Turner A.J., Billeter S., Terstegen F., Thiel S., Kendrick J., Rogers S.C., Casci J., Watson M., King F., Karlsen E., Sjøvoll M., Fahmi A., Schäfer A. and Lennartz C., QUASI: a general purpose implementation of the QM/MM approach and its application to problems in catalysis. *J. Mol. Struct.,* **632** (2003), 1–28.

[79] Neese F., Software update: the ORCA program system—version 5.0. *WIREs Comput. Mol. Sci.,* **12** (2022), e1606.

[80] Neese F., Software update: the ORCA program system—version 4.0. *WIREs Comput. Mol. Sci.,* **8** (2018), e1327.

[81] Neese F., The ORCA program system. *WIREs Comput. Mol. Sci.,* **2** (2012), 73–78.

[82] Smith W. and Todorov I.T., A short description of DL_POLY. *Mol. Simul.,* **32** (2006), 935–943.

[83] Smith W. and Forester T.R., DL_POLY_2.0: a general-purpose parallel molecular dynamics simulation package. *J. Mol. Graph.,* **14** (1996), 136–141.

[84] Kästner J., Carr J.M., Keal T.W., Thiel W., Wander A. and Sherwood P., DL-FIND: an open-source geometry optimizer for atomistic simulations. *J. Phys. Chem. A,* **113** (2009), 11856–11865.

[85] Van Santen J.A. and DiLabio G.A., Dispersion corrections improve the accuracy of both noncovalent and covalent interaction energies predicted by a density-functional theory approximation. *J. Phys. Chem. A,* **119** (2015), 6703–6715.

[86] Becke A.D., Density-functional thermochemistry. III. The role of exact exchange. *J. Chem. Phys.,* **98** (1993), 5648–5652.

[87] Caldeweyher E., Ehlert S., Hansen A., Neugebauer H., Spicher S., Bannwarth C. and Grimme S., A generally applicable atomic-charge dependent London dispersion correction. *J. Chem. Phys.,* **150** (2019), 154122.

[88] Weigend F. and Ahlrichs R., Balanced basis sets of split valence, triple zeta valence and quadruple zeta valence quality for H to Rn: design and assessment of accuracy. *Phys. Chem. Chem. Phys.,* **7** (2005), 3297.

[89] Roe D.R. and Cheatham T.E. III, PTRAJ and CPPTRAJ: software for processing and analysis of molecular dynamics trajectory data. *J. Chem. Theory Comput.,* **9** (2013), 3084–3095.

[90] Kisselev A.F. and Goldberg A.L., Proteasome inhibitors: from research tools to drug candidates. *Chem. Bio.,* **8** (2001), 739–758.

[91] Van de Donk N.W.C.J., Carfilzomib versus bortezomib: no longer an ENDEAVOR. *Lancet Oncol.,* **18** (2017), 1288–1290.

[92] Liu J., Zhao R., Jiang X., Li Z. and Zhang B., Progress on the application of bortezomib and bortezomib-based nanoformulations. *Biomolecules,* **12** (2022), 51.